

Geosynchronous Magnetopause Crossings in February–April 2023

A. V. Dmitriev*

Skobeltsyn Institute of Nuclear Physics, Moscow State University, Moscow, 119899 Russia

*e-mail: dalex@srd.sinp.msu.ru

Received August 15, 2023; revised September 9, 2023; accepted September 11, 2023

Abstract—Geosynchronous magnetopause crossings (GMCs) were analyzed during geomagnetic storms on February 26, March 23, and April 23, 2023. GMC-associated magnetosheath intervals were identified using magnetic data acquired from the *GOES-16* and *GOES-17* spacecraft. A comparative analysis of various magnetopause models was performed on the base of solar wind conditions measured by the *THEMIS-E* spacecraft and the *Wind* interplanetary monitor. The analysis of models was based on statistical parameters for determining magnetosheath intervals. It was shown that for all three storms, the model presented in [1] demonstrated the best accuracy. For events of moderate magnetic storms against the background of small negative B_z component of the interplanetary magnetic field (IMF), good results are obtained with the model described in [2]. For extreme events with very high solar wind pressures and/or very strong negative IMF B_z , the model shown in [3] exhibits good accuracy, and satisfactory accuracy is also demonstrated by models presented in [4, 5]. It was shown that the accuracy of the models was affected by the following factors and effects: the choice of interplanetary monitor, the dependence of the model on the solar wind pressure, the B_z saturation effect, the dawn–dusk magnetopause asymmetry, and the effect of prehistory.

DOI: 10.1134/S001095252360035X

INTRODUCTION

The problem of predicting intersections with the magnetopause of the geostationary orbit remains relevant at the present time [6]. Geostationary magnetopause crossings (GMCs) occur when the magnetosphere approaches Earth at geocentric distances of less than 6.6 Earth radii (R_E), causing geostationary satellites to enter the magnetosheath and even the interplanetary medium [7]. In practical terms, this implies the spacecraft venturing beyond the magnetosphere, which leads to a loss of orientation due to the magnetic field and the impact of dense plasma flows, as well as energetic particles of solar and heliospheric origin. This can result in damage or even loss of geostationary satellites [8–11]. Furthermore, understanding the dynamics of the magnetopause under strongly disturbed interplanetary and geomagnetic conditions observed during GMCs allows a deeper understanding of the interaction between the solar wind and the magnetosphere.

By the present time, a variety of models have been developed to predict GMCs under interplanetary conditions [2–5, 12, 13]. These models take into account various nonlinear effects that do not manifest in the magnetopause dynamics under unperturbed conditions. One such effect is the so-called “saturation of the impact” of the negative B_z component of the interplanetary magnetic field (IMF). Specifically, there is a saturation threshold for the impact of IMF B_z on the magnetopause, below which the magnetopause no

longer responds to further intensification of a large negative B_z [4, 12, 14, 15].

Another effect is the morning–evening asymmetry of the magnetopause [14, 16]. It involves the magnetopause shifting toward the evening for large negative IMF B_z , causing GMCs to be more frequently observed in the afternoon sector under the same conditions. The asymmetry effect is considered in only some models [1–3, 5].

Yet another effect is the prehistory [17], i.e., the dependence of the magnetopause response not only on current, but also on previous conditions in the interplanetary environment. The prehistory effect was proposed to explain false predictions of the magnetosphere during the initial phase of magnetic storms when all models confidently predicted GMCs, but geostationary satellites did not observe them. This effect is considered in the model of [3].

Several studies have been conducted for the comparative analysis of various GMC models during a series of magnetic storms [17–20]. These studies revealed a significant dispersion in the deviations of model predictions from observations during different storms. As a result, it has been challenging to determine the model with the best accuracy for GMC. This paper presents the results of a comparative analysis of several magnetopause models for predicting GMCs during magnetic storms on February 26, March 23, and April 23, 2023.

METHODS

Experimental Data

Satellite experimental data on key parameters of space plasma and the magnetic field were obtained from the CDAWeb database (<https://cdaweb.gsfc.nasa.gov/>). The analysis focuses on events when geostationary satellites observed the magnetopause. A GMC is defined as the moment when the spacecraft exits the magnetosphere into the magnetosheath and the moment it returns from the magnetosheath to the magnetosphere. Magnetic data from geostationary satellites *GOES-16* and *GOES-17* with a temporal resolution of 0.1 s were used for this purpose. The *GOES-16* and *GOES-17* spacecraft were located at geographic longitudes of 285° and 255°, crossing the local noon at 17:00 and 19:00 UT, respectively. The magnetosheath was identified as strong deviations in the magnetic field measured on the *GOES* spacecraft from the quasi-stationary geomagnetic field. Deviation is considered strong if the B_z component becomes negative or field intensity Bt becomes less than 100 nT. In this case, B_z on *GOES* does not necessarily have to be negative if the IMF B_z is positive. In the latter case, entry into the magnetosheath is caused by extremely strong solar wind pressure.

Data on the solar wind and IMF were obtained from the *Wind* interplanetary monitor and *THEMIS-E* spacecraft. The *Wind* monitor is located more than 200 R_E from Earth toward the Sun. The data from *THEMIS-E* were used when the spacecraft entered the interplanetary medium before the shock front. On the *Wind* spacecraft, magnetic data from the MFI instrument and plasma data from the SWE instrument have a resolution of ~100 s. On *THEMIS*, data from the FGM instrument and plasma data from the ESA instrument in reduced mode have a resolution of ~3 s. The *ACE* spacecraft data were not used due to severe degradation of its plasma instrument.

The analysis also involved data on the *SYM-H* index with a resolution of 1 min obtained from the World Data Center in Kyoto (<https://wdc.kugi.kyoto-u.ac.jp/aeasy/index.html>). The *SYM-H* index, like the hourly *Dst*, is a measure of the intensity of the ring current, more precisely, its symmetric part, calculated with higher temporal resolution.

The connection of interplanetary conditions to the state of the magnetosphere, i.e., the time delay for measurements in the interplanetary medium, was determined in the first approximation based on the time of direct propagation of the solar wind. However, the time delay may vary with changes in the orientation of interplanetary structures. Refining alignment was performed based on two criteria [21]: (1) the main criterion, using cross correlation between solar wind pressure and *SYM-H*, and (2) the additional criterion, using correlation between B_z and B_y components of IMF with measurements in the magnetosheath on *GOES* spacecraft.

Due to the significant variation in temporal resolutions, time series of different parameters were scaled to a common resolution of 1 s. With this accuracy, magnetopause crossings were determined. For low resolutions, extrapolation of the current value to the next measurement moment was carried out. All vector quantities were presented in the fully aberrated GMC coordinate system [22], taking into account the velocity of the Earth's rotation around the Sun and the non-radial nature of the solar wind, which often accompanies GMCs [21].

Magnetopause Models

The study considers six models that have been previously successfully used for GMC determination [20]: the asymmetric KS model [1], the Sh model [4], the neural network DS model [5], the asymmetric Ch model [13], the three-dimensional Li model [2], and the predictive PM model [3]. The models are characterized by different dependences on various parameters.

In particular, the KS, Sh, and Ch models calculate geocentric distance to the magnetopause R_m as a function of cone angle Ca from the X axis, directed from Earth to the Sun, as well as dynamic solar wind pressure Pd and IMF component B_z in the GSM coordinate system:

$$R_m = F(Ca, Pd, B_z). \quad (1)$$

The Ch model takes into account the aberration effect of the magnetosphere due to the rotation of the Earth around the Sun. The KS model considers the asymmetry effect of the magnetosphere with negative IMF B_z , leading to a shift of the magnetopause towards the evening. The neural network DS model represents the quasi-three-dimensional shape of the magnetopause as a function of GSM latitude (GSMLat), longitude (GSMLon), Pd , and IMF components B_y and B_z in a GSM:

$$R_m = F(GSMLat, GSMLon, Pd, B_z, B_y). \quad (2)$$

The three-dimensional Li model represents the magnetopause as a function of GSMLat, GSMLon, Pd , B_z , IMF strength B , and angle of inclination of the Earth's dipole ψ :

$$R_m = F(GSMLat, GSMLon, Pd, B_z, B, \psi). \quad (3)$$

The predictive PM model allows calculating the total pressure required for GMC at a given point (GSMLat, GSMLon) as a function of IMF B_z and *Dst* variation:

$$Pmp = F(GSMLat, GSMLon, B_z, Dst). \quad (4)$$

Total solar wind pressure Psw is calculated as

$$Psw = Pd + Pt + Pm, \quad (5)$$

where dynamic pressure Pd accounts for the contribution of helium, Pt is the thermal pressure of the solar wind plasma, and Pm is the magnetic pressure of the IMF. If $Pmp < Psw$, the geostationary spacecraft should cross the magnetopause and enter the magnetosheath.

Statistical Analysis

The accuracy of the models is determined by statistical parameters proposed in previous works [19, 22]. Specifically, for each individual event, statistics HT , MT , FA , and CR (in seconds) are calculated based on the observations and model outputs, as shown in Table 1. For example, Hit time HT accumulates intervals when the geostationary satellite is in the magnetosheath, and model distance to the magnetopause Rm is less than distance to the satellite Rg . Miss time MT corresponds to the model's inability to indicate the satellite's entry into the magnetosheath. False Alarm time FA corresponds to the model's erroneous prediction of the magnetosheath. Correct Rejection time CR corresponds to the model's correct prediction of the satellite's position inside the magnetosphere. Obviously, the sum of all statistics equals the total duration of the analyzed interval in seconds:

$$N = HT + MT + FA + CR. \quad (6)$$

To compare models based on statistics HT , MT , FA , and CR , the following statistical parameters are calculated:

$$PCP = \frac{HT + CR}{N}. \quad (7)$$

Parameter PCP (Probability of Correct Prediction) indicates the capability of the model to correctly predict intervals when the satellite was in the magnetosheath and the magnetosphere: $PCP = 0$ means complete inability, and $PCP = 1$ means perfect prediction of all intervals.

$$POD = \frac{HT}{HT + MT}. \quad (8)$$

The parameter POD (Probability of Detection) shows the capability of the model to predict magnetosheath intervals: $POD = 0$ means complete inability, and $POD = 1$ means perfect prediction of all magnetosheath intervals.

$$FAR = \frac{FA}{HT + FA}. \quad (9)$$

The parameter FAR (False Alarm Rate) indicates how often the model makes mistakes in predicting magnetosheath intervals: $FAR = 0$ means no false predictions of the magnetosheath, and $FAR = 1$ means all predictions of magnetosheath intervals are false.

$$OUR = \frac{MT - FA}{MT + FA}. \quad (10)$$

The parameter OUR (Overestimation Underestimation Ratio) shows the balance of the model. If the model systematically overestimates the distance to the magnetopause, OUR approaches 1. Obviously, for such a model, FAR will be relatively small, but POD will also be low. For a model that systematically underestimates the distance to the magnetopause, OUR approaches -1 . Such a model will have a high FAR ,

Table 1. Statistics table

	Magnetosheath	Magnetosphere
$Rm < Rg$	HT	FA
$Rm \geq Rg$	MT	CR

but also a large POD . For a balanced model, OUR is close to 0.

RESULTS

In the first half of 2023, GMCs were observed in the geostationary orbit by the *GOES-16* and *GOES-17* satellites during three events coinciding with the main phase of magnetic storms on February 26, March 23, and April 23. The main phase of these storms occurred in the second half of the day, providing conditions for observing GMCs on the *GOES-16* and *GOES-17* satellites.

Event on February 26, 2023

The magnetic storm of February 26, 2023, was moderate ($\min Dst = -69$ nT). It began with an SSC at 19:23 UT and reached its maximum at 22:30 UT. GMCs were observed by *GOES-17* from 20:44 to 21:10 UT, with a total time in the magnetosheath of 488 s. Figure 1 shows the moments of intersections, interplanetary and geomagnetic conditions, and model outputs for this interval. During this time, *GOES-17* was in the postnoon sector around 14:00 LT. *GOES-16* was rather far from noon, around 16:00 LT, and, therefore, did not observe GMCs.

Interplanetary conditions were measured by the *Wind* spacecraft, for which the time delay was about 49 min. Figure 1 presents an overview of the conditions. In reality, the time delay varied depending on the solar wind speed and the orientation of interplanetary structures. Therefore, the entire interval was divided into 10-min sectors, and the time delay was determined for each sector.

Figure 1 shows strong variations in IMF components B_z and B_y , accompanied by high solar wind pressure $P_{sw} > 12$ nPa. According to the classification provided in [23], this geo-effective structure is typical for a compressed interplanetary layer of the Sheath type, which forms behind the interplanetary shock wave ahead of the fast magnetic cloud (MC) associated with a coronal mass ejection from the Sun. Thus, in this case, the GMC was caused by high P_{sw} against a very strong varying IMF B_z in the region of the interplanetary structure of the Sheath type.

As seen in Fig. 1, the intervals of the magnetosheath are characterized by strong deviations of the magnetic field measured on the *GOES* satellite from the quasi-stationary geomagnetic field. In the interval from 20:45 to 20:55 UT, the B_z values on the *GOES*

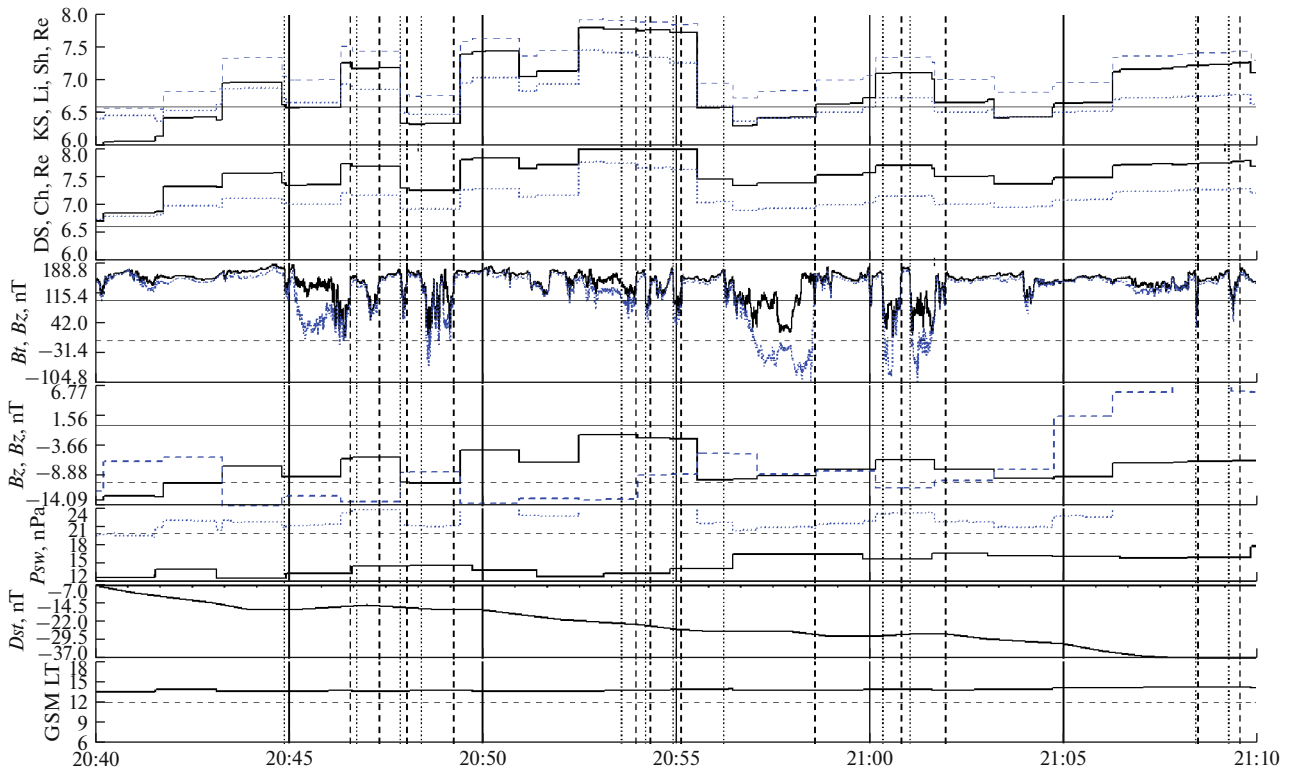


Fig. 1. Geosynchronous magnetopause crossings (GMCs) on February 26, 2023, based on geostationary *GOES-17* data and interplanetary conditions from the *Wind* spacecraft (panels top to bottom): distance to the magnetopause according to the KS (solid curve), Li (blue dashed curve), and Sh (blue dotted curve) models; distance to the magnetopause according to the DS (solid curve) and Ch (blue dashed curve) models; *GOES-17* data on the total magnetic field (solid curve) and GSM B_z component; GSM components of the IMF B_z (solid curve) and B_y (blue dotted curve); total solar wind pressure P_{sw} (solid black curve) and pressure required for the GMC according to the PM model (blue dashed curve); Dst variation of the geomagnetic field; *GOES-17* local time in aberrated GSM coordinates. Vertical dashed and dotted lines denote the GMC, exit and return to the magnetosphere, respectively. The time shift for the *Wind* spacecraft data is 49 min.

satellite were predominantly positive, while the IMF B_z was negative. This may be due to the fact that the *Wind* spacecraft observed another structure of the solar wind that did not reach Earth. In general, the magnetosheath was observed when solar wind pres-

sure P_{sw} was high, varying from 13.5 to 17 nPa; IMF B_z varied from -10 to -2 nT; and $SYM-H$ index varied from -14 to -37 nT.

The top two panels of Fig. 1 show the distances to the magnetopause calculated by various models. It is evident that the Sh, Ch, and DS models systematically overestimate the distance to the magnetopause and, therefore, cannot predict GMCs. A similar situation occurs with the PM model, which systematically overestimates the solar wind pressure required for GMCs. The accuracy of various models is presented by statistical parameters in Table 2 in the first rows. For models with systematic overestimation, statistical parameters $OUR = 1$, $FAR = 0$, and $POD = 0$; i.e., in this case, these models degenerate. Among the others, the KS and Li models demonstrate the highest accuracy. The interval from 20:40 to 20:43 UT should be noted, when these models underestimate the distance to the magnetopause and show a false magnetosheath interval. This may be due to the imperfections of the models as well as the different structure of the solar wind observed by the *Wind* spacecraft.

This assumption can be verified using data from the *THEMIS-E* spacecraft obtained just before the bow

Table 2. Statistical characteristics of models for February 26, 2023

Model	<i>OUR</i>	<i>FAR</i>	<i>PCP</i>	<i>POD</i>
KS-Wi	0.114	0.726	0.585	0.507
KS-TH	-0.856	0.646	0.567	0.957
Sh-Wi	0.925	1.000	0.744	0.000
Sh-TH	-0.136	0.608	0.661	0.726
Ch-Wi	1.000	0.000	0.774	0.000
Ch-TH	0.778	0.404	0.786	0.365
DS-Wi	1.000	0.000	0.774	0.000
DS-TH	1.000	0.000	0.774	0.000
Li-Wi	-0.238	0.706	0.553	0.699
Li-TH	-0.991	0.695	0.449	0.997
PM-Wi	1.000	0.000	0.774	0.000
PM-TH	0.995	1.000	0.756	0.000

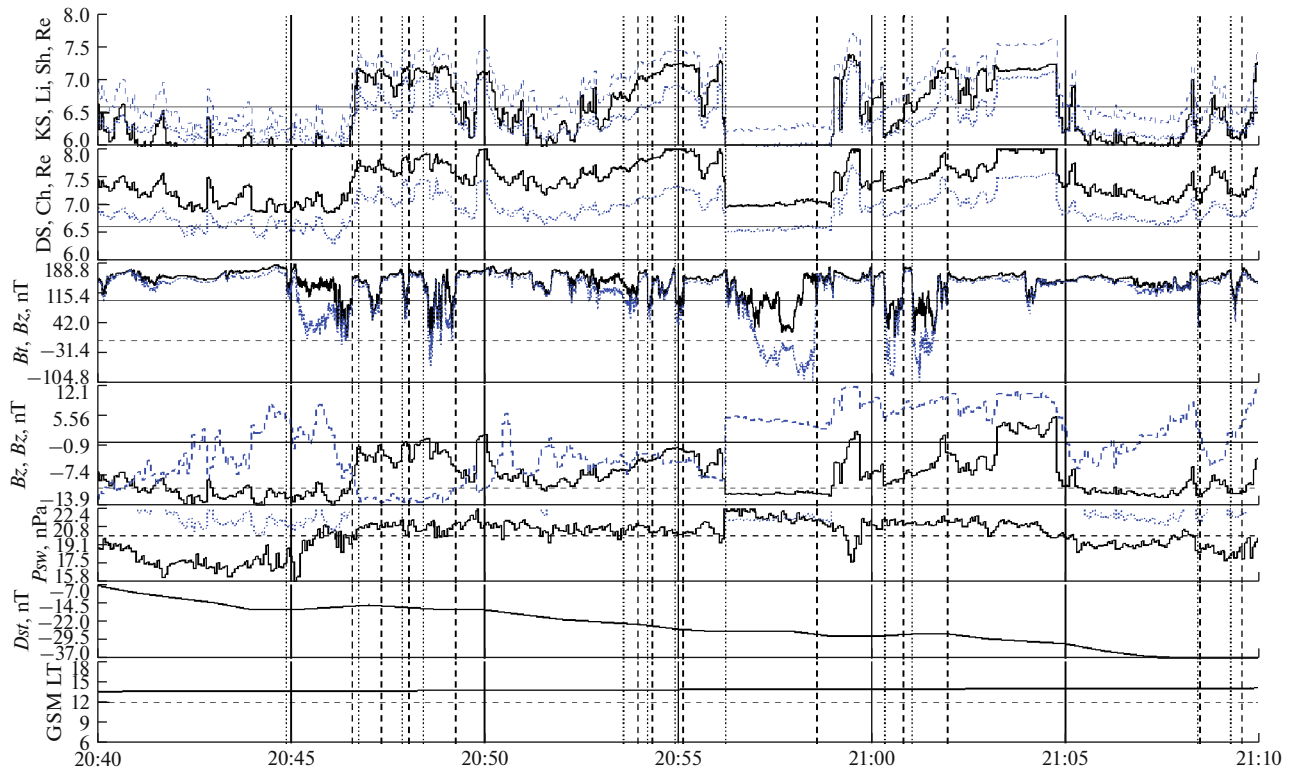


Fig. 2. Same as Fig. 1, but the interplanetary parameters were measured on the *THEMIS-E* spacecraft with a time shift of 1 min.

shock, as shown in Fig. 2. The conditions in this region are slightly different, so the magnetosheath was observed at pressures P_{sw} from 15.8 to 22.4 nPa, while IMF B_z varied from -13.9 to $+3$ nT. Higher pressure and strong negative IMF B_z in the interval from 20:40 to 20:45 UT caused false magnetosheath intervals in the KS, Sh, Ch, and Li models. Thus, in this case, there is an imperfection in the models, consisting in underestimating the distance to the magnetopause with strong negative B_z at the early stage of magnetic storm development when the ring current is not yet developed, and the Dst variation is small. This effect is taken into account in the PM model, which did not show a false magnetosheath. A similar situation is observed in the intervals from 20:50 to 20:55 UT and 21:05 to 21:03 UT when the KS, Sh, and Li models also show a false magnetosheath, and the PM model does not. On the other hand, almost all models, except DS, performed well in the magnetosheath interval from 20:56 to 20:59 UT when the solar wind pressure exceeded 22 nPa, and B_z dropped below -10 nT.

Statistical parameters for various models are presented in Table 2 in the second rows. In this case, the Sh model demonstrates the highest accuracy with a good balance (OUR close to 0) and high PCP , although its POD is not as high as in the KS and Li models. However, these models in this case strongly underestimate the distance to the magnetopause, manifested in a large negative OUR and relatively high

FAR . The highest $PCP = 0.786$ and low $FAR = 0.404$ are demonstrated by the Ch model; however, it has a relatively high percentage of overestimating the distance to the magnetopause ($OUR = 0.778$), leading to weak predictions of magnetosheath intervals with the lowest $POD = 0.365$. Considering all statistical characteristics, it can be concluded that, for this event, the best models are KS, Sh, and Li.

Event on March 23, 2023

The magnetic storm of March 23, 2023, was an initial intensification ($\min Dst = -70$ nT) of a strong storm, which started with an SSC at 06:00 UT and reached its maximum at 14:41 UT. On this day, data from the *GOES-17* satellite are not available. GMCs were observed by the *GOES-16* satellite in the pre-noon sector around 09:00 LT in a short interval from 14:12 to 14:30 UT, with a total magnetosheath time of 421 s, as shown in Fig. 3. During this period, the *THEMIS* spacecraft was in the magnetosheath.

Interplanetary conditions were measured by the *Wind* spacecraft, and the time delay for them was 49 min. As seen in Fig. 3, magnetosheath intervals are characterized by a large negative B_z . In general, the magnetosheath was observed when the solar wind pressure P_{sw} was very high, ranging from 16.5 to 30 nPa, IMF B_z varied from -8 to 0 nT, and Dst was around -35 to -44 nT. The magnetosheath intervals

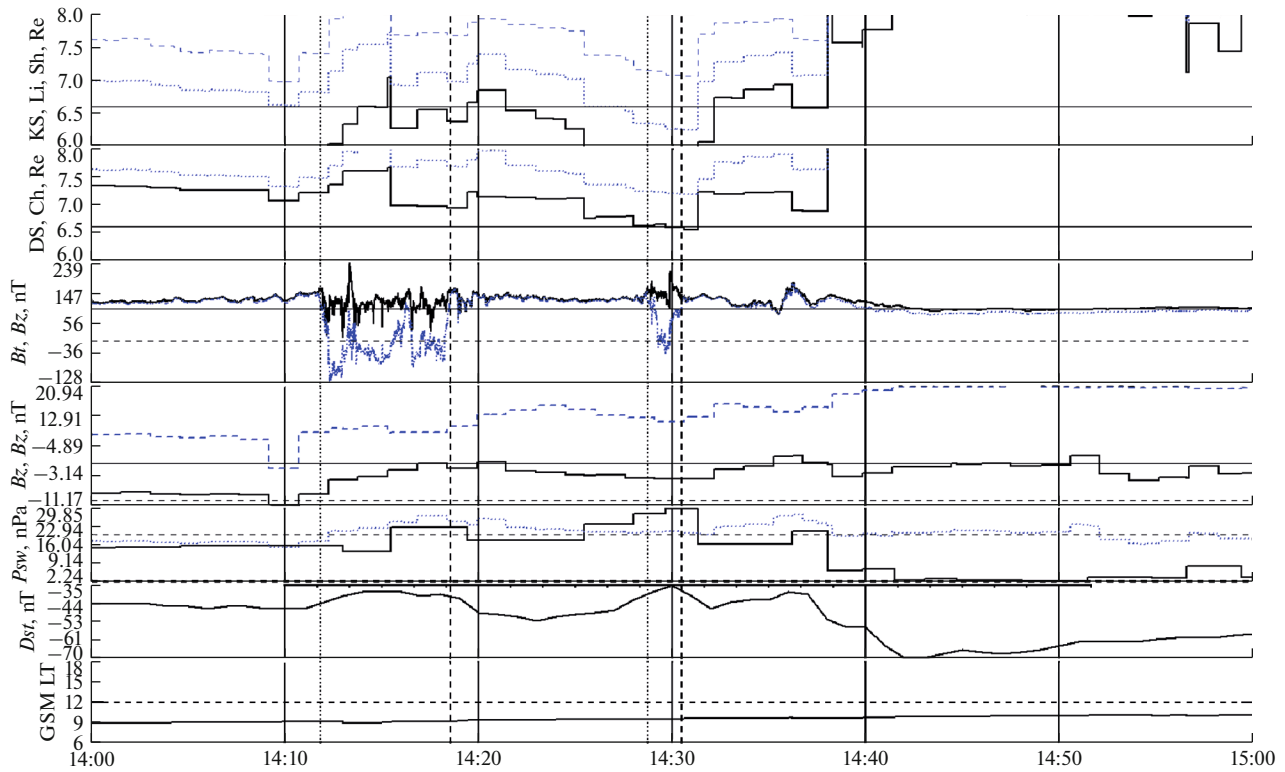


Fig. 3. Same as Fig. 1, but for March 23, 2023. Time shift is 51 min.

ceased after 14:32 UT when the solar wind pressure P_{sw} dropped almost 15-fold in 10 min from 30 to 2 nPa. The sharp decrease in P_{sw} against weak B_z is manifested in a large negative excursion in the $SYM-H$ index, from -35 nT at 14:30 UT to -70 nT at 14:41 UT; thus, it was not an intensification of the ring current [7]. The close correlation between P_{sw} and $SYM-H$ proves the correctness of the selected time delay. As in the previous event, the characteristic dynamics of IMF components and solar wind pressure indicate that GMCs are associated with conditions in the interplanetary structure of the Sheath type.

It can be seen in Fig. 3 that the first magnetosheath interval from 14:11:19 to 14:18:33 UT was predicted only by the KS model. The second short interval at a very high $P_{sw} = 30$ nPa from 14:28:45 to 14:30:29 was

predicted by the KS, Li, DS, and PM models. The Sh and Ch models systematically overestimated the distance to the magnetopause and did not show GMCs. According to the statistical parameters presented in Table 3, it can be concluded that all models are unbalanced (large $|OUR|$) in this event. The KS model provided the best accuracy for entering the magnetosheath, with $POD = 0.98$ and the lowest FAR . The Li and PM models also demonstrated reasonable accuracy with relatively high PCP and POD . Thus, in this case, the KS, Li, and PM models have the best accuracy.

Event on April 23, 2023

The magnetic storm on April 23, 2023, was a strong one ($\min Dst = -165$ nT). It began at 09:00 UT and reached its maximum at 22:00 UT. On that day, data from *GOES-17* are not available. GMCs were observed by *GOES-16* in the noon sector around 12:00–13:00 LT in the interval from 18:11 to 19:37 UT. The total time in the magnetosheath was 3586 s. Magnetosheath intervals and interplanetary and geomagnetic conditions, as well as model readings, are shown in Fig. 4. Interplanetary conditions were measured by the *Wind* spacecraft. The average time delay was 37 min. In reality, it varied depending on the solar wind speed and the orientation of interplanetary structures. Therefore, the entire interval was divided into 15-min sectors, and for each sector, an individual time delay was determined, ranging from 34 to 41 min.

Table 3. Statistical characteristics of models for March 23, 2023

Model	<i>OUR</i>	<i>FAR</i>	<i>PCP</i>	<i>POD</i>
KS-Wi	-0.946	0.595	0.436	0.980
Sh-Wi	1.000	0.000	0.571	0.000
Ch-Wi	1.000	0.000	0.571	0.000
DS-Wi	0.839	0.663	0.548	0.080
Li-Wi	0.428	0.702	0.472	0.249
PM-Wi	0.428	0.702	0.472	0.249

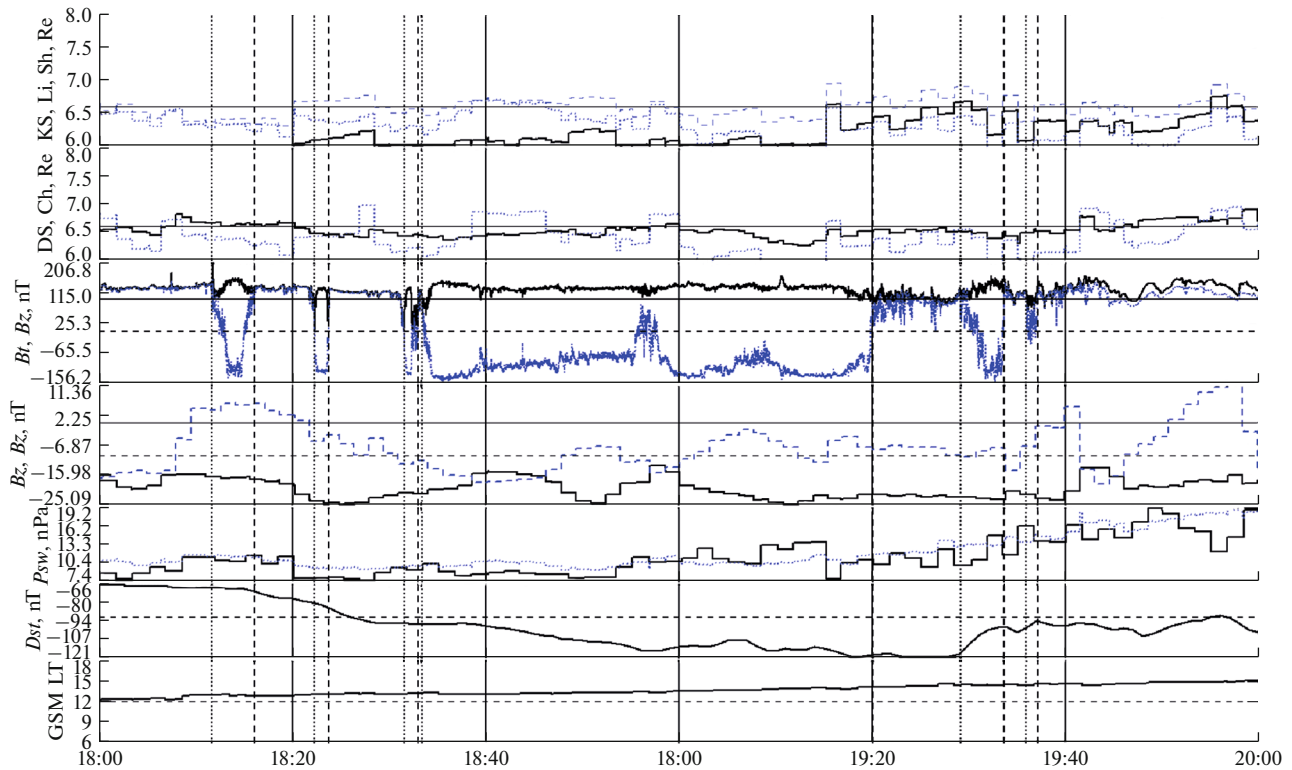


Fig. 4. Same as Fig. 1, but for April 23, 2023. Time shift is 37 min.

Magnetosheath intervals were observed against a very strong negative IMF B_z from -13 to -25 nT, resulting in large negative values of B_z measured by *GOES* in the magnetosheath. Solar wind pressure P_{sw} varied from 7.4 to 16.2 nPa, and the *SYM-H* index ranged from -69 to -121 nT. In Fig. 4, a prolonged and very strong negative IMF B_z is evident against a relatively low solar wind pressure P_{sw} of about 10 nPa, which is characteristic of interplanetary structures of the MC type [23].

In Fig. 4, it is seen that the models predict magnetosheath intervals quite well. However, the models also often show erroneous magnetosheath intervals, underestimating the distance to the magnetopause. Especially, the KS model significantly underestimates the distance. Statistical parameters of the models are compared in the first rows of Table 4. It is clear that all models, except Sh, are poorly balanced, and their $|OUR|$ is far from 0. The DS and PM models demonstrate the highest $PCP > 0.6$ and relatively low FAR . The KS, Ch, DS, and Li models show the highest accuracy for predicting magnetosheath intervals with $POD > 0.8$. It should be noted that the high POD of the KS model is due to a strong underestimation of the distance to the magnetopause. Overall, the KS, DS, and PM models have the best characteristics.

It is interesting to compare the model predictions based on the *THEMIS-E* data obtained just before the bow shock, as shown in Fig. 5. In this case, this region

features higher solar wind pressures ranging from 12 to 19 nPa and more extreme IMF B_z from -30 to -13 nT. More extreme conditions at the beginning and end of the interval from $18:00$ to $18:12$ UT and $19:36$ to $20:00$ UT caused false magnetosheath intervals for all models. It should be noted that two short intervals at $18:30-18:36$ UT and $19:27-19:30$ UT, when the *THEMIS-E* spacecraft was in the magnetosheath, were excluded from the analysis.

Table 4. Statistical characteristics of models for April 23, 2023

Model	<i>OUR</i>	<i>FAR</i>	<i>PCP</i>	<i>POD</i>
KS-Wi	-0.957	0.464	0.544	0.979
KS-TH	-0.915	0.430	0.569	0.958
Sh-Wi	-0.162	0.471	0.509	0.586
Sh-TH	-0.733	0.399	0.603	0.883
Ch-Wi	-0.582	0.448	0.555	0.809
Ch-TH	-0.912	0.419	0.586	0.959
DS-Wi	-0.735	0.402	0.630	0.898
DS-TH	-0.969	0.394	0.630	0.987
Li-Wi	-0.733	0.507	0.463	0.851
Li-TH	-0.994	0.433	0.569	0.997
PM-Wi	0.501	0.299	0.600	0.414
PM-TH	-0.532	0.374	0.620	0.809

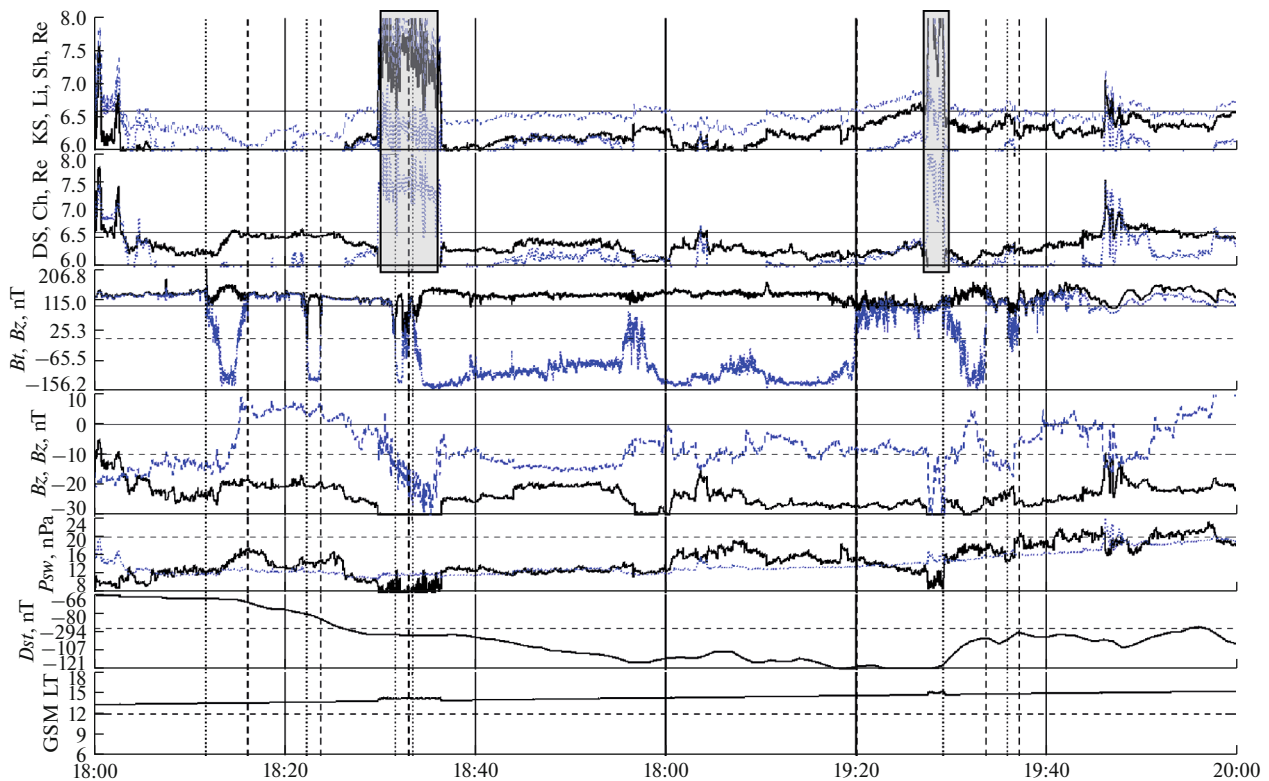


Fig. 5. Same as Fig. 1, but for April 23, 2023. The interplanetary parameters were measured on the *THEMIS-E* spacecraft with a time shift of 3 min. Gray rectangles indicate intervals when *THEMIS-E* was in the magnetopause.

The most extreme interplanetary conditions were observed from 18:36 to 19:30 UT when the *GOES-16* satellite was in the magnetosheath. It is important to note that, when IMF $B_z < 20$ nT, the KS, Sh, Ch, Li, and PM models do not respond to changes in B_z and follow variations in solar wind pressure P_{sw} . A notable example is the interval from 18:57 to 19:00 UT when the negative B_z dropped to maximum values of -30 nT. However, the models did not show a decrease in the distance to the magnetopause. On the contrary, they demonstrated a slight increase in distance, associated with a dip in P_{sw} , so that the Sh model even predicted a false return of the magnetosphere. This behavior of the models is explained by taking into account the saturation effect of the impact of IMF B_z near -20 nT.

For interplanetary data from the *THEMIS-E* spacecraft, statistical parameters of the models are presented in the second rows of Table 4. It is clear that, for all models, *OUR* has shifted to large negative values, which is associated with more extreme interplanetary conditions. The more or less balanced PM model, for which *OUR* remained at the level of 0.5, can be considered an exception. This model demonstrates high accuracy $PCP = 0.62$ and a record-low level of false predictions $FAR = 0.374$, although the prediction of the magnetosheath is not the best with $POD = 0.809$. Models KS, Ch, DS, and Li show high $POD > 0.9$. However, this is accompanied by a high level of false

predictions of the magnetosheath $FAR > 0.4$ and low accuracy $PCP < 0.6$. The DS model is an exception, with $FAR = 0.394$ and the highest accuracy $PCP = 0.63$. Thus, considering all statistical characteristics, the best models for interplanetary data from the *THEMIS-E* spacecraft are DS, PM, and Sh.

RESULTS AND DISCUSSION

Table 5 summarizes the general characteristics of interplanetary and geomagnetic conditions for all three events, and the best models for each event and interplanetary monitor are indicated. The event of February 26, 2023, is characterized by low storm activity and moderate solar wind disturbances with high solar wind pressures P_{sw} and large negative values of the IMF B_z . The models KS, Li, and Sh demonstrated the highest accuracy in predicting GMCs and magnetosheath intervals in this event. The event of March 23, 2023, is characterized by very high solar wind pressures, weak negative IMF B_z , and a relatively low level of geomagnetic activity. In this event, the KS, Li, and PM models showed good accuracy. It can be noted that both GMC events were associated with the arrival of an interplanetary magnetosheath, i.e., Sheath-type structures. In the event on April 23, 2023, magnetosheath intervals were observed against the background of strong storm activity and very strong nega-

Table 5. General characteristics of events and GMC models

Event	P_{sw} , nPa	B_z , nT	Dst , nT	Models	Structures
Feb. 26, 2023 <i>Wind</i>	13.5...17	-10...-2	-14...-37	KS, Li	Sheath
Feb. 26, 2023 <i>THEMIS</i>	15.8...22.4	-14...3	-14...-37	KS, Sh, Li	
March 23, 2023 <i>Wind</i>	16...29.9	-8...0	-35...-44	KS, Li, PM	Sheath
April 23, 2023 <i>Wind</i>	7.4...16.2	-25...-13	-69...-121	KS, DS, PM	MC
April 23, 2023 <i>THEMIS</i>	12...19	-30...-17	-69...-121	Sh, DS, PM	

tive IMF B_z , characteristic of an interplanetary structure of the MC type. In extreme conditions, the PM, DS, KS, and Sh models provided the highest accuracy.

Thus, the KS model demonstrated fairly high accuracy in predicting GMCs in all three events. The Li model predicts GMCs well in events with low storm activity and small negative IMF B_z . For extreme events with high pressures and/or very strong negative IMF B_z , the PM model showed good accuracy. The models Sh and DS predicted GMCs well during strong geomagnetic disturbances against the background of strong negative IMF B_z and high solar wind pressures.

Comparing models based on data from different interplanetary monitors, it is necessary to consider their distance from Earth, due to the presence of small-scale structures in the solar wind. Obviously, data from near-Earth monitors are more preferable. In addition, the degradation of plasma instruments should be taken into account when calculating solar wind pressure. As is evident in Table 5, the modern *THEMIS* spacecraft, launched in 2007, shows about 20% higher P_{sw} than the *Wind* spacecraft, launched in 1994. It should be noted that the main bulk of GMCs were analyzed and modeled using interplanetary data from the *Wind* and *ACE* monitors. By now, their plasma instruments have degraded, especially on the *ACE* spacecraft. Therefore, additional calibration of plasma data from distant interplanetary monitors with data from near-Earth spacecraft like *THEMIS* is required.

The ability to predict GMCs is also determined by the model's quality and its dependence on interplanetary parameters. In particular, it has been shown that the Sh model tends to overestimate the distance to the magnetopause during GMC [18], which results in a low FAR but also leads to a low level of magnetosheath prediction POD and a large positive OUR . Under normal conditions, on the contrary, the model underestimates the distance to the magnetopause [24]. This is due to the unbalanced dependence of the model on solar wind pressure.

Another problematic aspect is the saturation effect of the dependence of the distance to the magnetopause on the IMF B_z . In the Ch model, the saturation threshold depends on solar wind pressure [13]; in the PM model, it depends on the level of geomagnetic activity [3]; and, in the DS model, it has a complex

dependence on P_{sw} and B_y . However, this problem is still poorly researched. Therefore, the KS, Sh, and Li models introduce a threshold as a constant near $B_z = -20$ nT. In this case, the saturation effect was well manifested during extreme interplanetary conditions in the event of April 23, 2023 (Fig. 5), when the KS, Sh, Li, and PM models did not respond to changes in large negative IMF B_z , following only variations in solar wind pressure.

The accuracy of models also depends on unaccounted effects. One of them is the morning–evening asymmetry for GMCs with large negative IMF B_z [16]. This effect is strongly overestimated in the KS and DS models, causing them to systematically underestimate the distance to the magnetopause in the morning and noon sectors with strong negative IMF B_z . This leads to large negative OUR and increased FAR , although it ensures a high level of magnetosheath interval prediction POD .

Another problematic effect is the prehistory effect [17]. It is well known that the current state of the magnetosphere is determined by the integral dynamics of interplanetary conditions. In particular, Dst variation is an integral function of the impact of the induced electric field of the solar wind [25]. The PM model uses $SYM-H$ as a 1-min analogue of Dst variation, which can be considered a parameter depending on prehistory. As seen in Table 5, taking this effect into account indeed allowed avoiding the prediction of false magnetosheath intervals, lowering FAR , and improving the accuracy of the model at the initial phase of magnetic storms.

In summary, it can be said that the strong spread in the deviations of model predictions from observations of magnetosheath intervals related to GMCs is determined by both external and internal model factors. External factors include the quality of determining interplanetary conditions affecting the magnetopause. The model's dependences on interplanetary environment parameters and the current state of the magnetosphere are internal factors.

CONCLUSIONS

Based on the magnetic data from *GOES-16* and *GOES-17*, intervals were identified when geostationary satellites entered the magnetosphere during mag-

netic storms on February 26, March 23, and April 23, 2023. For these events, a comparative analysis of various magnetopause models was conducted using data from the *THEMIS-E* and *Wind* spacecraft. It was demonstrated that the *Wind* monitor observes interplanetary conditions that can significantly differ from those observed by the near-Earth *THEMIS-E* spacecraft. Comparison of models, based on statistical parameters for defining magnetosphere intervals, yielded the following results.

(1) The asymmetric model KS [1] demonstrated high accuracy for all three events [1].

(2) In events with low storm activity against a backdrop of small negative values of IMF B_z , the three-dimensional model Li [2] showed good results.

(3) For extreme events with very high solar wind pressures and/or very strong negative IMF B_z , the PM model [3] exhibited high accuracy.

(4) At high solar wind pressures and large negative IMF B_z , good accuracy was demonstrated by the models Sh [4] and the neural network model DS [5].

Based on the comparative analysis, it was shown that the accuracy of the models is influenced by the following factors and effects:

(1) dependence on solar wind pressure;

(2) saturation effect of the impact of large negative IMF B_z on the magnetopause;

(3) asymmetry of the magnetopause morning–evening during large negative IMF B_z ;

(4) prehistory effect.

Further development of GMC models should be based on a more careful consideration of these key factors and effects using both existing and new experimental data.

ACKNOWLEDGMENTS

The author is grateful to NASA/GSFC ISTP (<https://cdaweb.gsfc.nasa.gov/>) for providing data on the *Wind*, *GOES*, and *THEMIS* spacecraft. The author also thanks the Kyoto World Data Center for providing the *Dst* and *ASY/SYM* indexes (<https://wdc.kugi.kyoto-u.ac.jp/aesy/index.html>).

FUNDING

The study was carried out as part of the research topic “Sun Research, Monitoring and Modeling of the Radiation Environment and Plasma Processes in the Heliosphere and near-Earth Space.”

CONFLICT OF INTEREST

The author of this work declares that he has no conflicts of interest.

REFERENCES

1. Kuznetsov, S.N. and Suvorova, A.V., An empirical model of the magnetopause for broad ranges of solar wind pressure and B_z IMF, *Polar Cap Boundary Phenomena. NATO ASI Ser.*, 1998, vol. 509, pp. 51–61. https://doi.org/10.1007/978-94-011-5214-3_5
2. Lin, R.L., Zhang, X.X., Liu, S.Q., et al., A three-dimensional asymmetric magnetopause model, *J. Geophys. Res.*, 2010, vol. 115, p. A04207. <https://doi.org/10.1029/2009JA014235>
3. Dmitriev, A.V., Suvorova, A.V., and Chao, J.-K., A predictive model of geosynchronous magnetopause crossings, *J. Geophys. Res.*, 2011, vol. 116, p. A05208. <https://doi.org/10.1029/2010JA016208>
4. Shue, J.-H., Song, P., Russell, C.T., et al., Magnetopause location under extreme solar wind conditions, *J. Geophys. Res.*, 1998, vol. 103, no. A8, pp. 17691–17700. <https://doi.org/10.1029/98JA01103>
5. Dmitriev, A.V. and Suvorova, A.V., Three-dimensional artificial neural network model of the dayside magnetopause, *J. Geophys. Res.*, 2000, vol. 105, pp. 18909–18918. <https://doi.org/10.1029/2000JA900008>
6. Dredger, P.M., Lopez, R.E., and Collado-Vega, Y.M., Comparing magnetopause predictions from two mhd models during a geomagnetic storm and a quiet period, *Front. Astron. Space Sci.*, 2023, vol. 10, p. 1213331. <https://doi.org/10.3389/fspas.2023.1213331>
7. Dmitriev, A.V., Suvorova, A.V., Chao, J.-K., et al., Anomalous dynamics of the extremely compressed magnetosphere during 21 January 2005 magnetic storm, *J. Geophys. Res. Space Phys.*, 2014, vol. 119, pp. 877–896. <https://doi.org/10.1002/2013JA019534>
8. Lanzerotti, L.J., LaFleur, K., MacLennan, C.G., et al., Geosynchronous spacecraft charging in January 1997, *Geophys. Res. Lett.*, 1998, vol. 25, no. 15, pp. 2967–2970. <https://doi.org/10.1029/98GL00987>
9. Wrenn, G.L., Rodgers, D.J., and Ryden, K.A., A solar cycle of spacecraft anomalies due to internal charging, *Ann. Geophys.*, 2002, vol. 20, pp. 953–956. <https://doi.org/10.5194/angeo-20-953-2002>
10. Odenwald, S.F. and Green, J.L., Forecasting the impact of an 1859-caliber superstorm on geosynchronous Earth-orbiting satellites: Transponder resources, *Space Weather*, 2007, vol. 5.
11. Choi, H.-S., Lee, J., Cho, K.-S., et al., Analysis of GEO spacecraft anomalies: Space weather relationships, *Space Weather*, 2011, vol. 9, p. S06002. <https://doi.org/10.1029/2006SW000262>
12. Kuznetsov, S.N. and Suvorova, A.V., Solar wind control of the magnetopause shape and location, *Radiat. Meas.*, 1996, vol. 26, no. 3, pp. 413–416.
13. Yang, Y.-H., Chao, J.K., Dmitriev, A.V., et al., Saturation of IMF B_z influence on the position of dayside magnetopause, *J. Geophys. Res.*, 2003, vol. 108, no. A3. <https://doi.org/10.1029/2002JA009621>
14. Kuznetsov, S.N. and Suvorova, A.V., Shape of the magnetopause near geostationary orbit, *Geomagn. Aeron.*, 1997, vol. 37, no. 3, pp. 1–11.
15. Kuznetsov, S.N., Suvorova, A.V., and Dmitriev, A.V., Shape and dimensions of the magnetopause: Relation-

- ship with parameters of the interplanetary medium, *Geomagn. Aeron.*, 1998, vol. 38, no. 6, pp. 7–16.
16. Dmitriev, A.V., Suvorova, A.V., Chao, J.K., et al., Dawn-dusk asymmetry of geosynchronous magnetopause crossings, *J. Geophys. Res.*, 2004, vol. 109, p. A05203.
<https://doi.org/10.1029/2003JA010171>
 17. Shue, J.-H., Song, P., Russell, C.T., et al., Toward predicting the position of the magnetopause within geosynchronous orbit, *J. Geophys. Res.*, 2000, vol. 105, p. 2641.
<https://doi.org/10.1029/1999JA900467>
 18. Shue, J.-H., Song, P., Russell, C.T., et al., Dependence of magnetopause erosion on southward interplanetary magnetic field, *J. Geophys. Res.*, 2001, vol. 106, no. A9, pp. 18777–18788.
<https://doi.org/10.1029/2001JA900039>
 19. Yang, Y.-H., Chao, J.K., Lin, C.-H., et al., Comparison of three magnetopause prediction models under extreme solar wind conditions, *J. Geophys. Res.*, 2002, vol. 107, no. A1.
<https://doi.org/10.1029/2001JA000079>
 20. Dmitriev, A.V., Lin, R.L., Liu, S.Q., et al., Model prediction of geosynchronous magnetopause crossings, *Space Weather*, 2016, vol. 14, pp. 530–543.
<https://doi.org/10.1002/2016SW001385>
 21. Suvorova, A.V., Dmitriev, A.V., Chao, J.-K., et al., Necessary conditions for the geosynchronous magnetopause crossings, *J. Geophys. Res.*, 2005, vol. 110, p. A01206.
<https://doi.org/10.1029/2003JA010079>
 22. Dmitriev, A.V., Chao, J.K., and Wu, D.-J., Comparative study of bow shock models using *Wind* and *Geotail* observations, *J. Geophys. Res.*, 2003, vol. 108, no. A12.
<https://doi.org/10.1029/2003JA010027>
 23. Yermolaev, Yu.I., Yermolaev, M.Yu., Nikolaeva, N.S., et al., Interplanetary conditions for CIR-induced and MC-induced geomagnetic storms, *Bulg. J. Phys.*, 2007, vol. 34, pp. 128–135.
 24. Case, N.A. and Wild, J.A., The location of the Earth's magnetopause: A comparison of modeled position and in situ cluster data, *J. Geophys. Res. Space Phys.*, 2013, vol. 118, pp. 6127–6135.
<https://doi.org/10.1002/jgra.50572>
 25. Burton, R.K., McPherron, R.L., and Russell, C.T., An empirical relationship between interplanetary conditions and *Dst*, *J. Geophys. Res.*, 1975, vol. 80, pp. 4204–4214.

Translated by M. Chubarova

Publisher's Note. Pleiades Publishing remains neutral with regard to jurisdictional claims in published maps and institutional affiliations.